Journal of Anatomy

REVIEW

Novel morphological features of developing white matter pericytes and rapid scavenging of reactive oxygen species in the neighbouring endothelia

Samuel Quimby and Robert Fern

Department of Cell Physiology and Pharmacology, University of Leicester, Leicester, UK

Abstract

Capillary endothelia and pericytes form a close morphological arrangement allowing pericytes to regulate capillary blood flow, in addition to contributing to vascular development and support. Vascular changes associated with oxidative stress are implicated in important pathologies in developing whiter matter, but little is known about the vascular unit in white matter of the appropriate age or how it responds to oxidative stress. We show that the ultrastructural arrangement of post-natal day 10 (P10) capillaries involves the apposition of pericyte somata to the capillary inner basement membrane and penetration of pericyte processes onto the abluminal surface where they form close connections with endothelial cells. Some pericytes have an unusual stellate morphology, extending processes radially from the vessel. Reactive oxygen species (ROS) were monitored with the ROS-sensitive dye 2′,7′-dichlorofluorescin (DCF) in the endothelial cells. Exposure to exogenous ROS (100 μM H_2O_2 or xanthine/xanthine oxidase), evoked an elevation in intracellular ROS that declined to baseline during the ongoing challenge. A second challenge failed to evoke an intracellular ROS rise unless the nerve was rested for > 4 h or exposed to very high levels of exogenous ROS. Exposure to a first ROS challenge prior to loading with DCF also prevented the intracellular ROS rise from a second challenge, proving that dye washout during exposure to ROS is not responsible for the loss of a second response. Perfusion with 30 μM extracellular Ca^{2+} or the voltage-gated Ca^{2+} antagonist diltiazem partially prevented this rapid scavenging of intracellular ROS, but blocking either catalase or glutathione peroxidase did not. The phenomenon was present over a range of post-natal ages and may contribute to the high ROS-tolerance of endothelial cells and act to limit the release of harmful ROS onto neighbouring pericytes.

Key words: brain; capillaries; ischaemia; micro-vessels; pericyte; reactive oxygen species; white matter.

Introduction

Pericytes form a close morphological arrangement with the endothelial lining of brain capillaries (Sims, 1986; Shepro & Morel, 1993). They are important for the formation and maintenance of the blood-brain barrier (Gerhardt & Betsholtz, 2003; Persidsky et al. 2006), for providing physical support to capillaries (Daneman et al. 2010) and for local haemodynamic regulation (Metea & Newman, 2006; Peppiatt et al. 2006). Pericyte processes wrap around capillary endothia and can fuse with the inner basement membrane and align directly parallel to the endothelial cell membrane. Retinal capillaries have the most extensive pericyte coverage in the body and injury to retinal pericytes is implicated in important diseases of the visual system such as diabetic retinopathy and retinopathy of prematurity (Motiejunaite & Kazlauskas, 2008). In diabetic retinopathy, hyperglycaemia associated with cellular reactive oxygen species (ROS) generation are thought to be important pathways to endothelia and pericyte cell death (Mustapha et al. 2010). A low pericyte density in the germinal matrix is associated with elevated vascular fragility and may contribute to germinal matrix–intraventricular haemorrhage, a leading cause of developmental brain injury (Braun et al. 2007). The major pathology associated with the developing brain is selective white matter damage associated with ischaemia and infection (Back & Rivkees, 2004). Despite these considerations, little is known about the features of the pericyte–endothelial relationship in immature white matter or their response to ROS.

Correspondence

Robert Fern, Department of Cell Physiology & Pharmacology, University of Leicester, P.O. Box 138, University Road, Leicester, LE1 9HN, UK. T: +44 (0)116 2523098; E: RF34@le.ac.uk

Materials and methods

All procedures involving the use of animals were approved by local ethical review. Optic nerves were dissected from neonatal Lister hooded rats and placed in aCSF composed of (in mM) 153 Na^+, 3 K^+, 2 Mg^{2+}, 2 Ca^{2+}, 131 Cl^-, 26 HCO_3^-, 2 $H_2PO_4^-$, 10 dextrose, bubbled with 95% O_2/5% CO_2 (pH 7.45). The majority of experiments were performed on nerves from P8–P12 rats (called 'P10' throughout). At this age, the optic nerve is initiating the process of myelination, with the first wraps of myelin appearing (Vaughn, 1969; Foster et al. 1982). The post-natal period in optic nerve development is characterized by rapid maturation of axon myelination and glial cell development (Skoff et al. 1976; Hildebrand & Waxman, 1984; Small et al. 1987), while micro-vascular development appears to be largely complete by postnatal day 14 (Scott & Foote, 1984). The preparation is therefore at a similar developmental point to the human periventricular white matter, which is subject to injury in the fetus at risk of cerebral palsy (Back et al. 2001; Craig et al. 2003). Ca^{2+} solutions with a free Ca^{2+} concentration of 30 μM contained 90 μM ethylene glycol-bis[β-aminoethyl ether]-N,N,N',N'-tetraacetic acid (EGTA) and 120 μM of added $CaCl_2$ (Salter & Fern, 2005). The presence of trace Ca^{2+} in the deionized water used for this solution may result in slight deviation from the calculated value. Catalase (250 U mL^{-1}) was purchased from Calbiochem (Merck, UK). Unless otherwise stated, all chemicals were purchased from Sigma-Aldridge (UK). Data are presented as mean ± SEM, with statistical significance determined by ANOVA with Tukey post-test (PRISM, Graphpad Software, San Diego, CA, USA).

ROS imaging

The ROS-sensitive fluorescent dyes 6-carboxy-2',7'-dichloro-dihydrofluorescein diacetate (6C-H_2-DCFDA) and 2',7'-dichloro-dihydrofluorescein diacetate (H_2-DCFDA) (Molecular Probes, Invitrogen, UK) were used to assess changes in ROS levels in neonatal rat optic nerve. These dyes are membrane-permeable and are de-esterified in the cytoplasm into the ionized free acids (H_2-DCFDA to 2',7'-dichloro-dihydrofluorescein and 6C-H_2-DCFDA to 6-carboxy-2',7'-dichloro-dihydrofluorescein), which will react with ROS present in the cytoplasm to form fluorescent 2',7'-dichloro-dihydrofluorescein (DCF) or 6-carboxy-2'7'-dichlorofluorescein (6C-DCF), respectively. H_2-DCFDA and 6C-H_2-DCFDA were dissolved in dry dimethylsulphoxide (DMSO) and 10% pluronic acid and loaded into nerves at a final concentration of 2 μM for 10 min. Optic nerves were maintained in hydrated 95% O_2/5% CO_2 atmosphere during the incubation period and were washed in aCSF before being mounted in a perfusion chamber. The ends of the optic nerves were fixed to a 22 × 40 mm glass coverslip with small amounts of cyanoacrylate glue, leaving the majority of the nerve completely free of glue (see Thomas et al. 2004). The coverslip was sealed onto a Plexiglas perfusion chamber (atmosphere chamber, Warner Instruments, Hamden, CT, USA) with silicone grease. aCSF was perfused through the chamber at a rate of 2–3 mL min^{-1}, with a fluid level of ∼ 2 mm completely covering the optic nerve. 95% O_2/5% CO_2 was blown over the aCSF at a rate of 0.3 L min^{-1}. The chamber was mounted on the stage of a Nikon Eclipse TE200 inverted epifluorescence microscope. Chamber temperature was maintained close to 37 °C with a flow-through feedback tubing heater (Warner Instruments) positioned immediately before the aCSF

entered the chamber, and a feedback objective heater (Bioptechs, Butler, PA, USA) that warmed the objective to 37 °C. This combination of heating systems regulated the temperature of the bath and coverslip to 37 °C, as established periodically with a temperature probe. Nerves were illuminated between 470 and 490 nm by monochromator (Optoscan; Cairn Research, Faversham, UK), and images were collected at 520 nm using an appropriate filter set (Chroma Technology, Rockingham, VT, USA). Images were taken with a cooled CCD camera (CoolSNAP HQ, Roper Scientific, Trenton, NJ, USA) every 60 s. Data were collected and stored with the image acquisition program META-FLUOR (Universal Imaging, Downingtown, PA, USA) running on Windows XP.

Unlike loading with AM-masked lipophilic dyes such as FURA-2, FURA-FF, BCECF or SBFI (Fern, 1998; Thomas et al. 2004), the acetate-masked H_2-DCFDA and 6C-H_2-DCFDA did not segregate into glial cells in the neonatal nerves. The wide-field fluorescence emanating from the optic nerves that was used for imaging was rather diffuse at rest, and occasional micro-vessels were the only clear cellular components. As individual cells were not apparent in the resting nerve, we collected data from large regions of whole optic nerves that will include micro-vessels, glia and axons. As 2',7'-dichloro-dihydrofluorescein and 6-carboxy-2',7'-dichloro-dihydrofluorescein are trapped within cells while the fluorescent products are not, this signal will reflect intracellular ROS changes. The amplitude of responses was calculated from the mean peak value (averaged over a 5-min period) relative to the projected baseline adjusted for drift.

Confocal imaging

Transgenic mice strain FVB/N-Tg(GFAPGFP)14Mes/J (JAX stock number 003257), carrying green fluorescent protein (GFP; hGFP-S65T) under the control of the human GFAP promoter, were used for confocal imaging of astrocytes (Shannon et al. 2007; Salter & Fern, 2008). Heterozygous males were mated with wild-type females and transgenic littermates identified at post-partum day 4 (P4) using a blue light source and appropriate filters (the transgenic animals exhibited a characteristic green glow around their eyes). Transgenic mice strain FVB/N, carrying the enhance GFP (EGFP) coding sequence under the control of mouse CNP promoters 1 and 2 (Yuan et al. 2002), were kindly donated by the laboratory of Vittorio Gallo (NIH, Bethesda, MD, USA) and were used for confocal imaging of oligodendroglial cells (Salter & Fern, 2005). Heterozygous males were mated with wild-type females and transgenic littermates identified. Mice were backcrossed to wild-type FVB/N females to the third generation to reduce GFP expression levels and eliminate a tendency to seizures in the litters. Optic nerves from transgenic animals were dissected out at P7-13 and sealed in an atmosphere perfusion chamber at 37 °C for imaging with an Olympus IX70 confocal microscope.

Electron microscopy

Ten RONS were collected, washed in Sorenson's buffer and post-fixed in 3% glutaraldehyde/Sorenson's. Nerves were then fixed with 2% osmium tetroxide and dehydrated prior to infiltration in epoxy. Ultrathin sections were counterstained with uranyl acetate and lead citrate and examined with a Jeol 100CX electron microscope. Glial cell processes could be identified on

ultrastructural grounds (Wilke et al. 2004). For example, the astrocyte process in Figs 1 and 2 clearly contains glial filaments. Pericytes can be positively identified as cells positioned between the inner and outer capillary basement membrane, or cells neighbouring the basement membrane and extending processes through the basement membrane. Microglial cells can be excluded using classic ultrastructural features and are largely absent at this stage of development in the rat optic nerve (see Wilke et al. 2004; Alix & Fern, 2009).

Results

The vascular unit of developing central white matter

The post-natal day 10 (P10) rat optic nerve is just starting the programme of myelination (Hildebrand & Waxman, 1984) and is a suitable model to examine vascular development in immature white matter. Examined at the ultrastructural level, blood vessels within the nerve always run longitudinally, parallel to surrounding axons. Rare larger vessels ($\sim$ 10 μm in diameter) lack smooth muscle tunica media and are largely covered in astrocyte processes that contact the outer layer of the basement membrane (Fig. 1). Pericytes are located between the inner and outer basement membrane layers and extend processes which penetrate the inner basement and directly contact the endothelial cell membrane. Features of these pericytes include a heterogeneous chromatin often lining the nuclei envelope and a wide-bore and extensive endoplasmic reticulum that appears to branch and is frequently studded with ribosomes. Mitochondria are apparent but not at high densities compared to metabolically active cells such as the neighbouring oligodendrocytes, which are starting to myelinate axons at this point (Fig. 1). Smaller capillaries (Fig. 2) are present at higher density and generally encompass a single endothelia cell somata or rim of endothelia cell processes. These vessels also run uniformly parallel to axons and can be very small ($\sim$ 2–3 μm) or somewhat larger (3–4 μm), the smaller of which may represent developing capillaries not yet capable of providing effective vascular supply. At this point in development, small capillary pericyte soma sometimes exhibit the classic morphology occupying the space between the inner and outer basement membrane and extending processes around the endothelia (Fig. 2A). Alternatively, pericyte somata may reside outside the basement membrane and have a more complex morphology, including processes that extend radically from the vessel to contact neighbouring glial soma and processes (Fig. 2B–E). These more stellate pericytes invariably extend processes which invade the basement membrane (Fig. 2D) to encapsulate the endothelia. A wide-bore, branched, rough endoplasmic reticulum is typical and can also be found in the abluminal processes (Fig. 2E, asterisks). Close connections can sometimes be observed between the pericyte processes and endothelial cells (Fig. 2C, arrows), which may represent gap-junctions. It is worth noting that such stellate pericytes
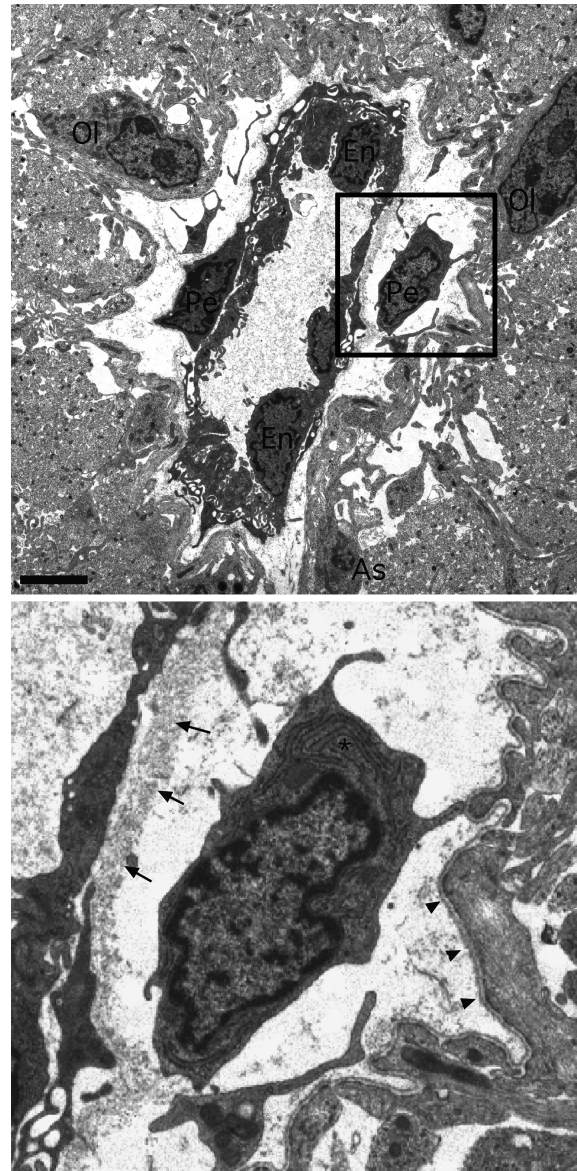

Fig. 1 Electron micrograph showing the morphological arrangement of a large P10 RON capillary (box shown at higher magnification below). The capillary lumen is 2–8 μm in diameter and is filled with plasma which appears grainy. The vessel is surrounded by astrocyte processes which cover the outer basement membrane, by axon profiles which are largely pre-myelinated and by oligodendroglial ('Ol') and astrocyte ('As') somata. Three endothelial somata ('En') and their processes line the lumen and are surrounded by an inner basement membrane (arrows). Two pericyte somata and their processes are located between the inner and outer (arrow heads) basement membrane. Pericyte inclusions include a wide-bore endoplasmic reticulum ('*'), mitochondria and cytoplasmic granules. Note the fine processes extending from the larger pericyte processes. Scale bar: 2 μm.

share no common features with microglial cells, which are very rare in the P10 rat optic nerve, contain convoluted narrow-bore endoplasmic reticulum, have large oval nuclei and an oval soma (see Alix & Fern, 2009).
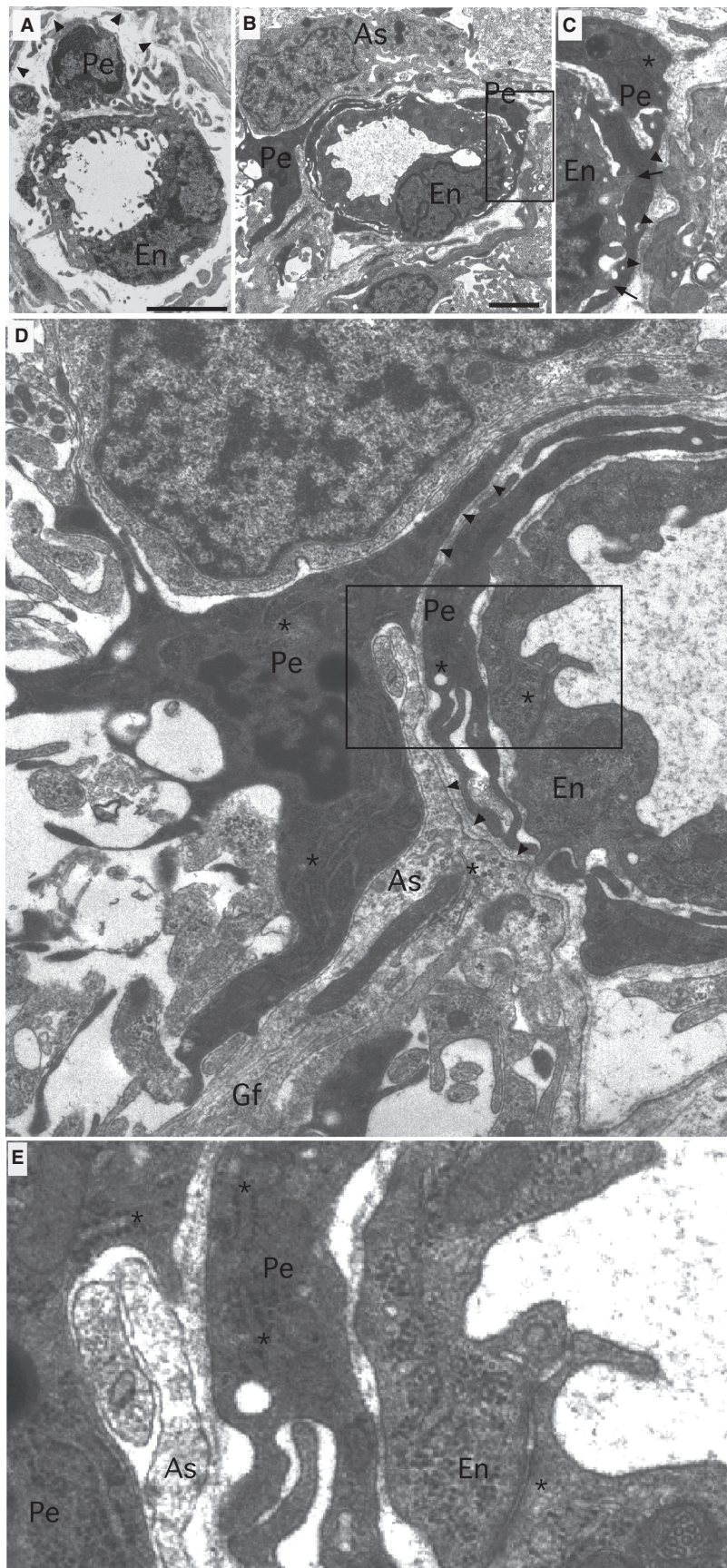
Significance of oxygen free radicals

A high polyunsaturated lipid content, coupled to a high rate of oxidative metabolism and a relatively low capacity for free-radical buffering, place the CNS at particular risk of attack by free radicals such as ROS (Sayre et al. 1999; Dringen et al. 2000). ROS are implicated in neurological diseases ranging from Alzheimer's to stroke (Traystman et al. 1991; Richardson, 1993), and may be particularly harmful in the developing brain during the evolution of the white matter lesions that underlie cerebral palsy. There is evidence both for elevated ROS levels in the CSF of neonates with selective white matter injury (Inder et al. 2002) and for free-radical-mediated cell damage in post-mortem sections (Back et al. 2005). Cells of the oligodendrocyte lineage suffer the greatest damage in these cases, and these cells have a heightened sensitivity to ROS attack and a reduced ability to buffer free radicals at the cellular level (Back et al. 1998). Endothelial cells of the brain vasculature are a rich potential source of ROS that may subsequently damage glial cells and axons (Zweier et al. 1988), and ROS-mediated injury of endothelial cells and their accompanying effects upon the blood-brain barrier may be important in a number of CNS pathologies (e.g. Mark & Davis, 2002; Lee et al. 2004).

The capacity of cells to scavenge ROS is largely determined by the concentration of cytoplasmic glutathione and the expression levels of the enzymes catalase, superoxide dismutase and glutathione peroxidase. Cellular stress responses to free radical attack can result in an increased expression of these defence mechanisms, occurring over a period of several hours (e.g. Ridnour et al. 2005), in addition to the *de novo* synthesis of a number of unidentified proteins (Wiese et al. 1995). These events can greatly increase cellular resistance to an exogenous ROS-like peroxide (H_2O_2) but the effect requires hours to evolve (Spitz et al. 1987; Wiese et al. 1995; Ridnour et al. 2005). We have developed an ROS-sensitive dye-loaded isolated whole-mount rodent optic nerve preparation to examine acute ROS handling in developing central white matter. We describe increased ROS scavenging in this preparation that is triggered within minutes of exposure to an exogenous ROS challenge. The phenomenon is partly dependent upon Ca^{2+} influx, does not appear to involve up-regulation of cat-

alase or glutathione peroxidase, and is too rapid to result from increased protein expression. The precise mechanism underlying the rapid ROS buffering response is not clear but the phenomenon is likely to be highly significant in a variety of clinical scenarios.

Evoked ROS changes

The application of ROS-sensitive dye imaging to a whole-mount preparation presents some technical challenges. Several reports suggest that DCF is the most sensitive dye to use and that good cell loading can be achieved by relatively brief periods of incubation with H_2-DCFDA (e.g. Keller et al. 2004). In the current experiments, DCFH-loaded nerves exhibited diffuse fluorescent emission under control conditions (Fig. 3A, left). As DCFH does not fluoresce, this indicated background production of DCF and therefore ROS in the tissue. Exposing nerves to 100 μM H_2O_2 resulted in an increase in fluorescence that was apparent largely in the nerve micro-vasculature and to a lesser degree throughout the nerve (Fig. 3A, middle). This fluorescence increase was not sustained during a 20-min period of exposure to 100 μM H_2O_2, and began to decline toward the end of the H_2O_2 challenge (Fig. 3A, right). DCFH cannot be fixed in tissue and dye localization to specific cell types within the preparation cannot be achieved by standard immuno-staining approaches. We therefore loaded neonatal optic nerves from transgenic mice that expressed GFP either in astrocytes (GFP-GFAP) or oligodendroglia (GFP-CNPase), representing the two major cell types present in the preparation. Because laser illumination itself produces oxidative stress (e.g. Tirlapur et al. 2001), scanning evoked significant DCF fluorescence in the live preparation that revealed the location of DCFH-loaded cells. As there is little separation between the excitation peaks of the forms of GFP available in these animals, DCF, GFP and DCF were separated via their emission spectra. Red emission following excitation at 488 nm revealed DCF largely restricted to micro-vessels within the nerve (Fig. 3B,C). These vessels were generally < 5 μm in diameter and endothelial cells lining the vessels clearly contained DCF. Astrocytes (green cells in GFP-GFAP mice), showed no DCF fluorescence, and only an occasional oligodendroglial cell (green cells in GFP-CNPase mice) contained DCF.

Fig. 2 Electron micrographs showing the typical morphological arrangement of small P10 RON capillaries. (A) A P10 RON capillary with a lumen diameter of 2–3 μm. The somata and processes of a single endothelial cell ('En') line the capillary lumen and the somata and processes of a pericyte ('Pe') are located under the basement membrane (arrowheads). (B,C) A P10 capillary with a luminal diameter of 3–4 μm (boxed area in B is shown in C). An endothelial cell is enclosed within a pericyte process under the basement membrane (C, arrowheads). The pericyte process makes close connections with the endothelia cell ('C', arrows). (D,E) Same section as B but at higher magnification. The pericyte somata is next to the capillary basement membrane and extends processes to nearby glial cells and their processes. A perivascular process merges with the basement membrane (D, arrowheads), while an astrocyte process (As) containing glial filaments (Gf) intervenes between the pericyte somata and the basement membrane. The boxed area in D is shown at higher gain in 'E', revealing that the pericyte contains wide-bore, rough, branched endoplasmic reticulum, while the endothelial cell contains narrow-bore, smooth, endoplasmic reticulum (*). The endothelia cell also contains numerous cytoplasmic granules and vesicular bodies. Scale bar: 2 μm.
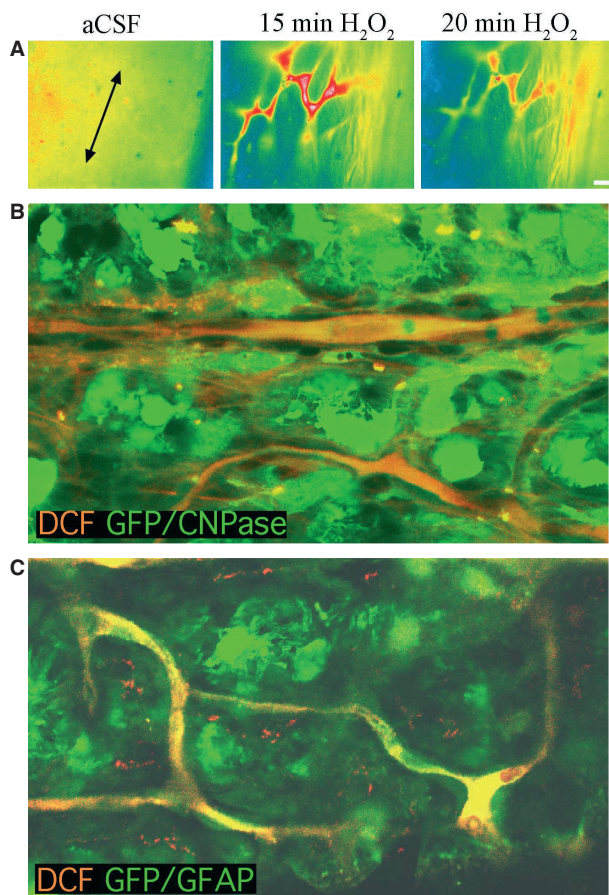
Fig. 3 ROS imaging and DCF localization in neonatal optic nerve. (A) Right: A typical wide-field image of the H2-DCDFD loaded P10 rat optic nerve. The long axis of the nerve is indicated by the arrows and the nerve edge is oriented to the right. Note the diffuse nature of the fluorescence in control conditions. Middle: The same region of nerve is shown after 15 min exposure to 100 μM H_2O_2. Note the bright fluorescence in structures that have the morphological appearance of nerve micro-vessels. Right: The same region of nerve after 20 min exposure to 100 μM H_2O_2. Note that the fluorescence has started to decline. (B) DCF localization in P10 GFP-CNPase mouse optic nerve. Top, left: DCF fluorescence collected via confocal imaging. Note that laser illumination has caused a rise in DCF in micro-vessels running through the nerve section. Bottom, left: The same section showing GFP within numerous oligodendrocytes, in addition to bleed-through of DCF fluorescence. Right: The images are overlaid, showing that the DCF-loaded endothelial cells of the nerve micro-vessels are distinct from the oligodendrocytes, which largely show no DCF fluorescence. (C) DCF localization in P10 GFP-GFAP mouse optic nerve. Top, left: DCF fluorescence collected via confocal imaging. Note that laser illumination has caused a rise in DCF in micro-vessels. Bottom, left: The same section showing GFP within numerous astrocytes, in addition to bleed-through of DCF fluorescence. Right: The images are overlaid showing that DCF-loaded endothelial cells of the nerve micro-vessels are distinct from the astrocytes, which show no DCF fluorescence. Scale bars: 10 μm. The wide-field DCF images have been pseudo-coloured to indicate fluorescent intensity.

As DCF fluorescence is dependent upon the reaction of DCFH with ROS, individual DCF-filled structures, micro-vessels and cells were not readily apparent at the start of experiments (Fig. 3A, left). To limit the production of ROS by the illumination, a relatively low rate of data collection was used and large regions of nerve were imaged. The recordings therefore correspond to changes in cytoplasmic ROS production largely, but not necessarily exclusively, within micro-vascular endothelial cells. Other than a variable degree of drift and noise, DCF fluorescence in nerves was stable during perfusion with aCSF, and was elevated following exposure to either a mixture of xanthine + xanthine oxidase (X + XO: giving rise to the $O_2^{.-}$ radical) or 100 μM H_2O_2 (giving rise to ·OH radical) (Fig. 4A,B). In both cases, the increase in cytoplasmic ROS that followed exposure to the exogenous ROS challenge was temporary and returned towards the baseline in the continued presence of exogenous ROS. Following washout, the re-application of the exogenous ROS failed to produce a rise in cytoplasmic ROS. The mechanism underlying this phenomenon was common to both species of radical, as application of X + XO prevented a subsequent exposure to H_2O_2 from affecting cytoplasmic ROS levels (Fig. 4C). The amplitude of DCF-fluorescence changes in response to exogenous ROS was highly variable and the mean peak response to a first and second exposure to 100 μM H_2O_2 is shown in Fig. 4D, excluding two outlying experiments that showed much bigger responses to a first application. Responses to a second application were not significantly different from baseline ($P > 0.05$).

Several tests were performed to investigate the apparent rapid increase in ROS scavenging apparent in Fig. 4. One possibility is that DCFH may be depleted from the nerve during the application of exogenous ROS, although the observation that the background DCF fluorescence returned close to the pre-exposure level rather than to zero suggests that this is unlikely. H_2-DCFDA-loaded nerves were therefore subjected to an ROS challenge prior to resting and subsequent exposure to a second ROS challenge. Various intervals between the two periods of ROS exposure were tested, revealing that the response to ROS recovered after 4–5 h (Fig. 5A–D). These findings are consistent with the presence of a rapidly induced form of ROS scavenging that lasts for several hours and cannot be explained in terms of dye loss from the preparation. To confirm this finding, nerves were pre-exposed to 100 μM H_2O_2 for 20 min in a Petri dish prior to washing with aCSF, loading with H_2-DCFDA and mounting for imaging. No elevation in DCF fluorescence was found using this protocol (Fig. 4E). To ensure that the transient loss of response to ROS in H_2-DCFDA-loaded nerves is not restricted to this dye, nerves were loaded with 6C-H_2-DCFDA, the fluorescent reaction product of which (6C-DCF) is more highly charged than DCF and which is retained to a greater degree within cells. Exposure to 100 μM H_2O_2 evoked a transient elevation in ROS which declined more slowly than that seen with the less charged reaction product DCF (Fig. 5E). To ensure that the 6C-H_2-DCFDA-loaded optic nerves were still capable of
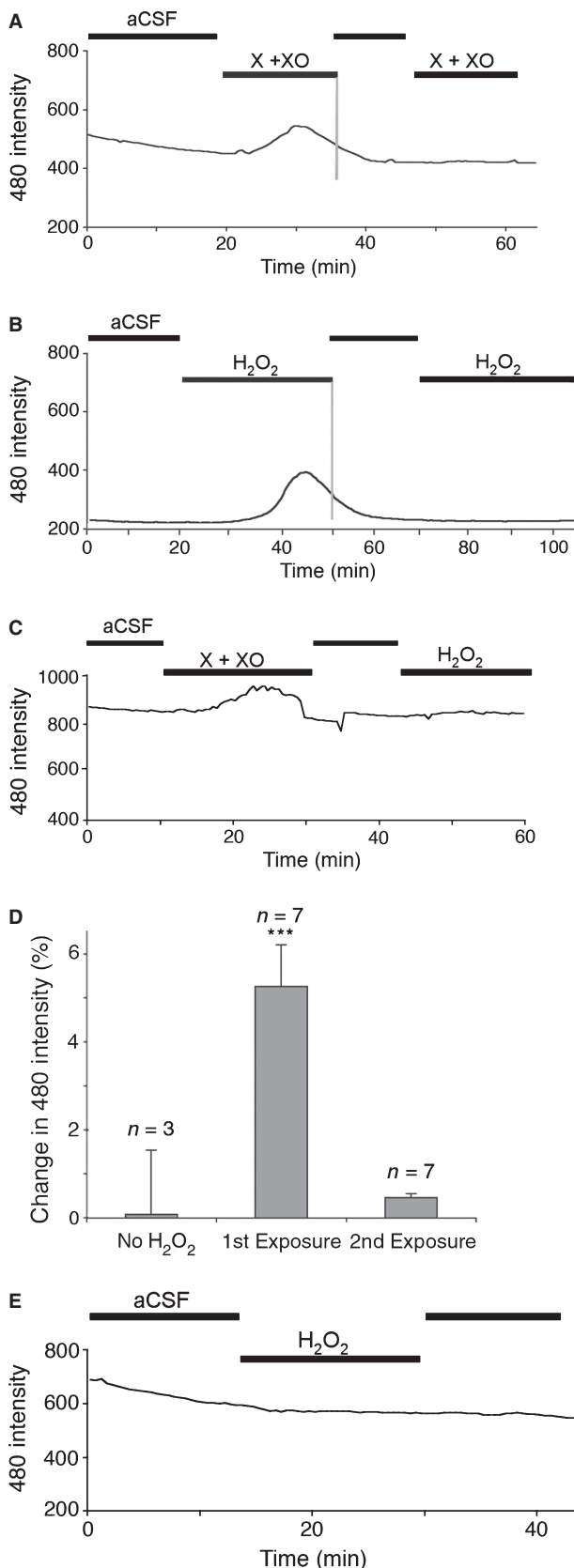
reporting an ROS increase they were subsequently exposed to a high concentration of H_2O_2 (10 mM), which also evoked a transient response (Fig. 5E).

The effect of lowering the extracellular $[Ca^{2+}]$ was examined. We have recently found that exposing P10 rodent optic nerve to very low or zero-Ca^{2+} conditions results in cell death and shedding of glial cell processes (Salter & Fern, 2005). We therefore exposed optic nerves to 30 μM Ca^{2+}, conditions that have no toxic action in this preparation at this age (Salter & Fern, 2005). H_2O_2 100 μM produced significantly larger responses in H_2-DCFDA-loaded optic nerves in 30 μM Ca^{2+} compared to responses produced in normal aCSF (Fig. 6A,B). In addition, when the time-course of the ROS rises were compared, ROS levels remained elevated for longer during H_2O_2 exposure in 30 μM Ca^{2+} (the mean rate of DCF fluorescent decline in normal aCSF is included in Fig. 6B in grey). Furthermore, unlike all experiments conducted in normal aCSF, a second exposure to 100 μM H_2O_2 produced a second, small amplitude rise in ROS (Fig. 6B, arrow). The calcium channel blocker diltiazem (50 μM) had a similar effect to that seen in 30 μM Ca^{2+} (Fig. 6A,C).

The role of H_2O_2 clearance was investigated by interfering with the major cellular enzymes responsible for H_2O_2 removal; catalase and glutathione peroxidase. Nerves were pre-exposed to either the catalase inhibitor 3-amino-1,2,4-triazole (3AT, 20 μM) or the glutathione peroxidase inhibitor mercaptosuccinic acid (MS, 10 mM), for 120 min prior to exposure to 100 μM H_2O_2. Under both conditions, 100 μM H_2O_2 evoked ROS rises that recovered to baseline in the continued presence of H_2O_2 (Fig. 7A,B). During catalase inhibition with 3AT, the amplitude of the response was significantly greater than in control nerves (Fig. 7C), which was not the case for MS-treated nerves.

We tested the effects of exogenous ROS upon nerves from rats of two age ranges in addition to the P10 animals

Fig. 4 Exogenous ROS evoke transient intracellular ROS rises in neonatal rat optic nerve. (A) Intracellular ROS levels are assessed as changes in DCF fluorescence (following excitation at 480 nm) in H2-DCDFD-loaded P10 optic nerve. There is a gradual decline in fluorescence with time in aCSF and an elevation following the application of xanthine + xanthine oxidase (X + XO). The fluorescent signal falls back to baseline in the continued presence of X + XO and a second application has no effect. (B) A similar series of events are seen in this optic nerve following the application of 100 μM H_2O_2. (C) An exposure to X + XO blocks any subsequent effect of H_2O_2 exposure. (D) Amplitude of DCF fluorescence changes in control nerves, following a first exposure to 100 μM H_2O_2 or following a second exposure (protocol as in Fig. 2B). ***$P < 0.001$ vs. control. (E) An optic nerve exposed to 100 μM H_2O_2 in a Petri dish for 20 min prior to washing; H2-DCDFD loading shows no response to a subsequent 100 μM H_2O_2 exposure. All data plots show single representative experiments.
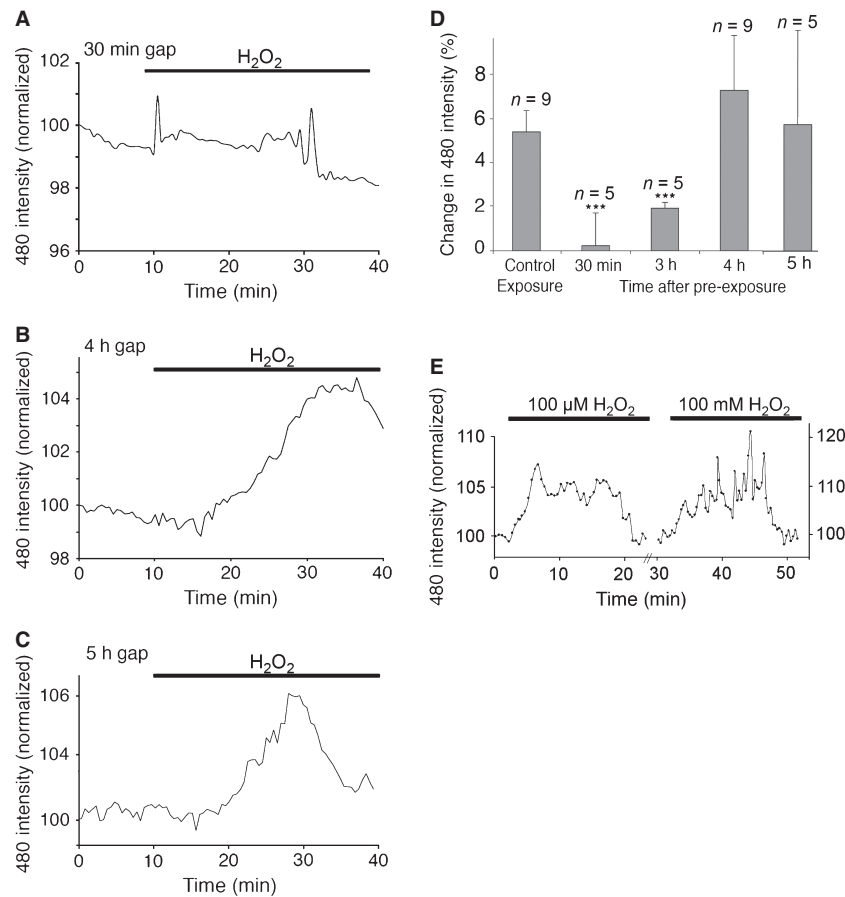
Fig. 5 Temporal features of rapid ROS scavenging. (A–C) Mean changes in DCF fluorescence evoked by 100 μM H_2O_2 at 30 min (A), 4 h (B) and 5 h (C) after an initial exposure (20 min 100 μM H_2O_2 in a Petri dish). Note the absence of response after 30 min and the recovery of response at 4 and 5 h. (D) Mean amplitude of responses to 100 μM H_2O_2 following a single, control 20-min exposure and at various times after a first exposure. ***$P < 0.001$ vs. control exposure. (E) Changes in 6C-DCF fluorescence in 6C-H_2-DCFDA-loaded nerves. Exposure to 100 μM H_2O_2 evoked an elevation in 6C-DCF fluorescence that declined to baseline levels in the continued presence of the exogenous ROS. Subsequent application of a high concentration of H_2O_2 (10 mM) evoked a similar transient 6C-DCF rise. All data plots show mean normalized responses.

already described. Perfusion with 100 μM H_2O_2 had no significant effect upon ROS levels in H_2-DCFDA-loaded nerves at either P3 (Fig. 8A; $P > 0.05$ vs. control, $n = 5$) or P20 (Fig. 8C; $P > 0.05$ vs. control, $n = 6$), indicating that the P10 nerve may be particularly sensitive to ROS perturbations. Higher concentration did evoke ROS rises at both P3 (Fig. 8B; 1 mM H_2O_2, $n = 5$) and P20 (Fig. 8D,E; 10 mM H_2O_2, $n = 6$). In both cases these rises declined to baseline in the continued presence of H_2O_2, indicating that rapid ROS scavenging is not restricted to a single point in white matter development.

Discussion

An ultrastructural description of pericytes in developing CNS white matter is not found in the literature, and little transmission electron microscopy data exists for pericytes of smaller CNS capillaries in general. In the P10 optic nerve, we found pericytes with a classical morphology, including a rounded soma with a large nucleus which was located under the outer basement membrane with processes surrounding the abluminal surface. Such pericytes were typical around larger vessels and were also found in smaller capillaries. We also found pericytes with a more complex morphology that could be described as 'stellate'. Stellate pericytes were found exclusively around smaller capillaries. These cells had somata outside the basement membrane but extended processes both through the basement membrane to the endothelial cell membrane to which close connection were made, and away from the vessel toward neighbouring glial cells. These cells contained more cytoplasm than 'classical' pericytes which was rich in rough endoplasmic reticulum. Presumably, these are immature cells that are involved in the maturation of their associated capillary, as such cells have never been reported in mature CNS. Stellate pericyte precursor cells of possible mesenchymal origin have been described in other tissue (Sims, 1986). We were able to distinguish these cells from microglia using well documented morphological criteria; microglial cells are known
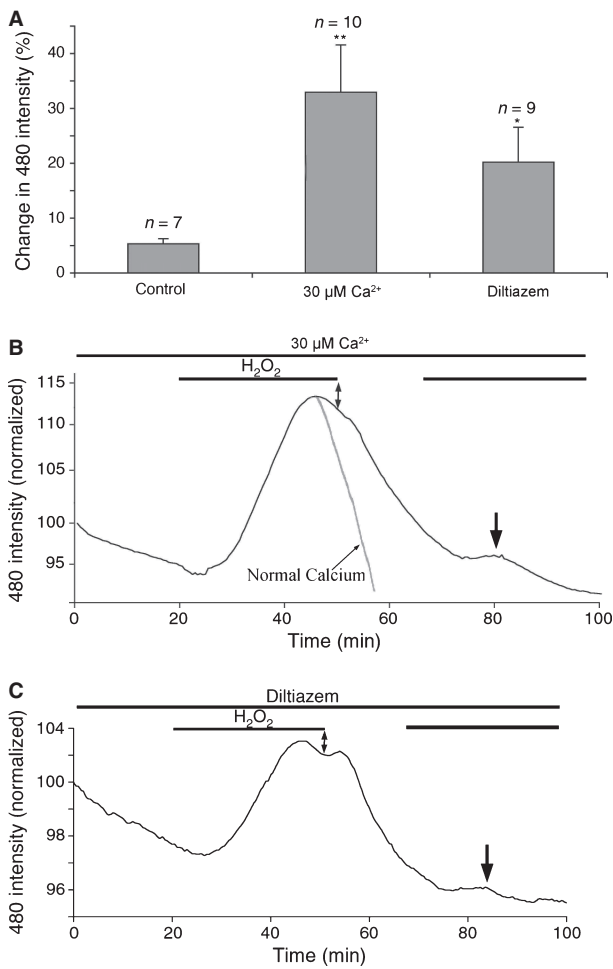
Fig. 6 Rapid ROS buffering is partly Ca^{2+}-dependent. (A) Mean change in DCF fluorescence in normal Ca^{2+}, 30 μM Ca^{2+}, and in the presence of the Ca^{2+} channel blocker diltiazem (50 μM). *$P < 0.05$ vs. control, **$P < 0.01$ vs. control. (B) The mean change in DCF fluorescence for nerves exposed to 100 μM H_2O_2 in 30 μM Ca^{2+}. Note that the fluorescence remains elevated in the continued presence of H_2O_2 (double arrow), and the response to a second exposure to H_2O_2 (arrow). The mean decline in normal Ca^{2+} is included for comparison, scaled to match (grey trace). (C) Similar plot for the mean DCF changes evoked by 100 μM H_2O_2 in the presence of diltiazem.

to be rare in at this stage in development in the optic nerve.

Having examined the morphological arrangement of the micro-vasculature in the rat optic nerve, we used the whole-mount isolated preparation to study ROS handling, which is key to vessel injury. The application of an extrinsic ROS challenge evoked a transient elevation in DCF fluorescence in H_2-DCFDA-loaded neonatal rat optic nerve. Membrane-permeable H_2-DCFDA is converted to DCFH within the cytoplasm, which can subsequently react with intracellular ROS such as the hydroxyl radical ($\cdot$OH) and peroxynitrate ($ONOO^-$) to produce fluorescent DCF, which is uncharged and can diffuse out of the cell (see Keller et al. 2004; Gomes et al. 2005). This allows both increases and
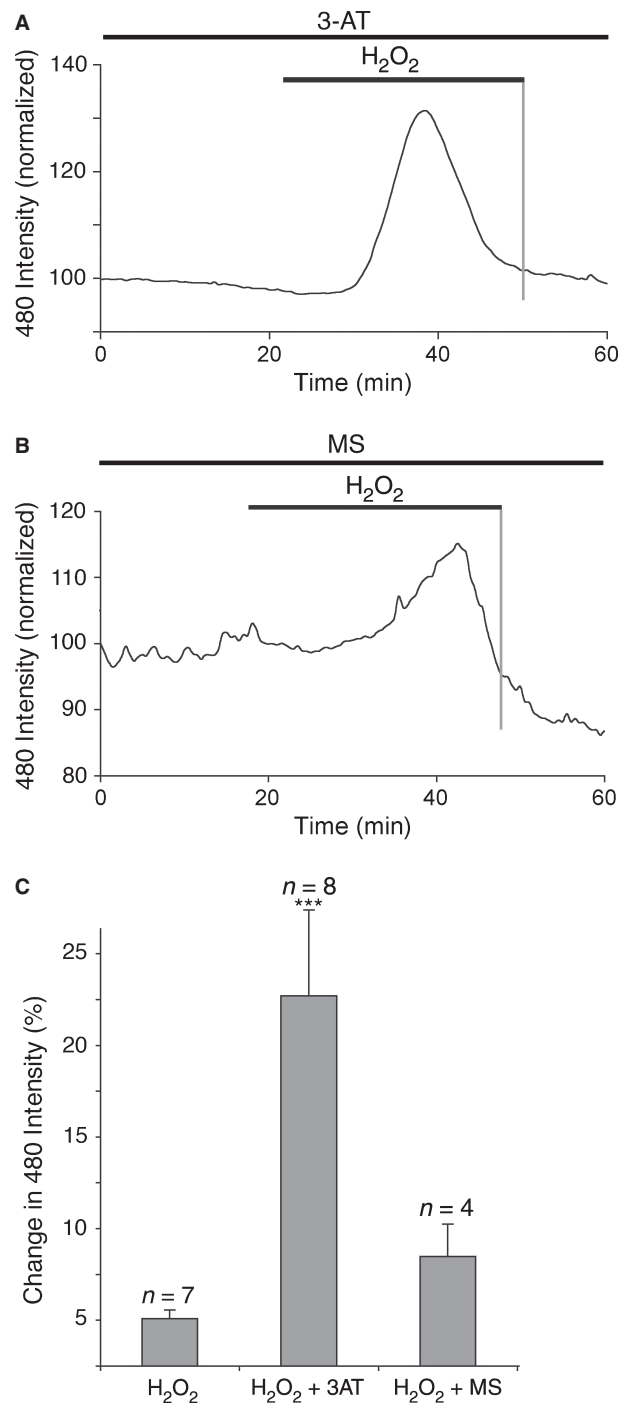

Fig. 7 Rapid ROS buffering is not blocked by catalase or glutathione peroxidase inhibitors. (A,B) The mean change in DCF fluorescence for nerves exposed to 100 μM H_2O_2 in the presence of the catalase inhibitor 3-AT (A, 20 μM) or the glutathione peroxidase inhibitor MS (B, 10 mM). (C) Mean changes in the peak response to 100 μM H_2O_2, showing a significant increase in the presence of 3-AT. ***$P < 0.001$ vs. H_2O_2 alone.

decreases in ROS concentration to be assessed with relatively high time resolution, as previously described within neural cells (e.g. Reynolds & Hastings, 1995; Safiulina et al.
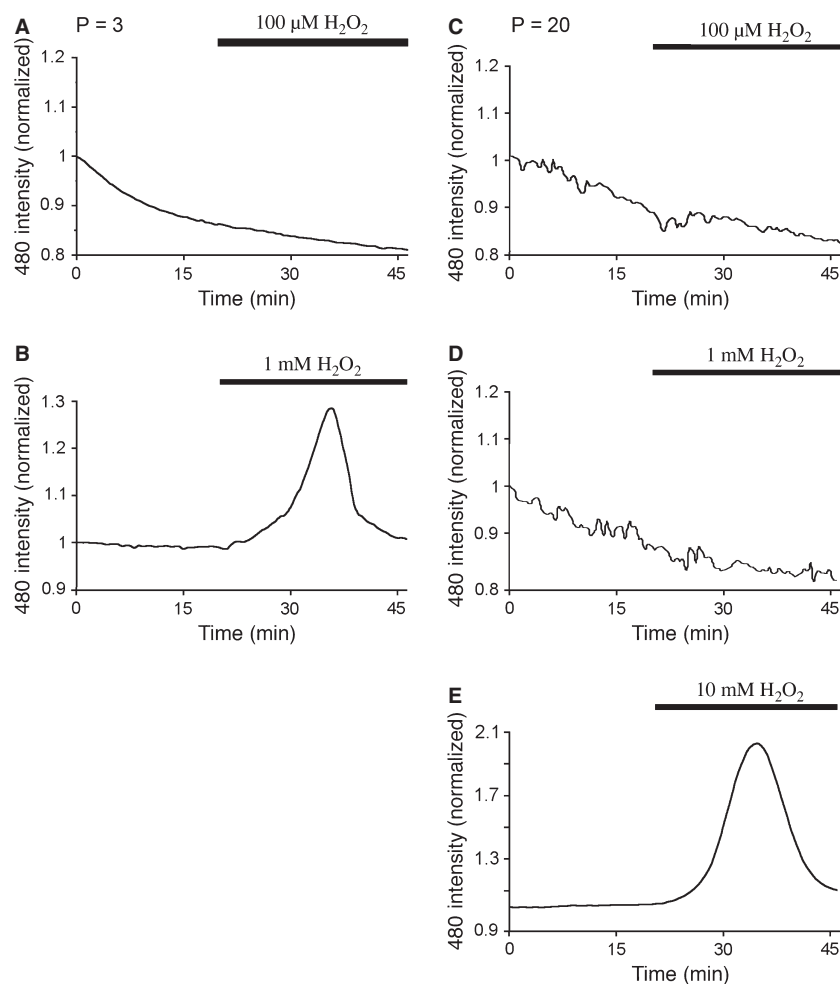
Fig. 8 Rapid ROS buffering is present at various points in white matter development. (A) Exposure to 100 μM H_2O_2 had no effect upon P3 optic nerve ROS levels. (B) Exposure to 1 mM H_2O_2 evoked an elevation in mean DCF fluorescence that was not maintained in the continued presence of the challenge. (C) 100 μM H_2O_2 had no effect on P20 optic nerve ROS levels. (D) 1 mM H_2O_2 had no effect on P20 optic nerve ROS levels. (E) 10 mM H_2O_2 evoked an elevation in mean DCF fluorescence that was not maintained in the continued presence of the challenge.

2006). Recording real-time ROS changes using dyes such as H_2-DCFDA in whole-mount preparations presented some technical challenges. While the cell type that has loaded DCFH can be reliable determined in cell culture studies, this is not the case in preparations such as the brain slice or the isolated optic nerve. DCFH cannot be fixed and so cell identification via standard immuno-staining approaches is not possible. Indeed, in the absence of a significant ROS load, DCFH-loaded cells do not fluoresce under control conditions. Using a short H_2-DCFDA-loading paradigm, we produced a preparation where DCF fluorescence during laser illumination was restricted largely to cells lining the microvessels of the nerve. Laser illumination at 488 nm will evoke a uniform ROS challenge (e.g. Tirlapur et al. 2001), and thus reveal the location of DCFH within the tissue. Animals with GFP expression linked to cell-specific promoters showed that DCFH-loaded cells were neither astrocytes nor oligodendrocytes. These glial cells are the only significant cell types in the nerve at this age other than pericytes and

endothelial cells. The rapid elevation and subsequent decline in DCF signal recorded from the optic nerve during a ROS challenge therefore arises largely from ROS changes in the vascular unit.

The apparent rapid-onset scavenging of ROS in white matter has not been described previously, and the findings must be interpreted with caution. We believe that the rapid loss of DCF fluorescence in neonatal optic nerve reported here in the continued presence of exogenous ROS is not an artifact arising from the methodology. The most obvious source of an artifact would be depletion of DCFH from the nerves during ROS application, leading to a run down in the generation of DCF with time. However, the background level of DCF fluorescence was not significantly altered by the period of exposure to ROS, while the response to ROS was absent from nerves that were pre-exposed to ROS prior to H_2-DCFDA loading. Furthermore, the response to ROS recovered over a 4-h period following the initial exposure, which is not compatible with loss of DCFH from the

preparation. An acid shift inside cells can reduce DCF fluorescence (Reynolds & Hastings, 1995; Mattiasson et al. 2003), although the likelihood of a profound, delayed pH change in the cells starting $\sim$ 15 min after the start of a ROS challenge and continuing for another 4 h is highly unlikely. Indeed, previous studies show either no pH change in endothelial cells upon exposure to H_2O_2, or a rapid acid shift of $\sim$ 0.1–0.2 pH units (Hu et al. 1998; Sipos et al. 2005). pH changes in this range will have no significant effect upon DCF fluorescence (Mattiasson et al. 2003).We suggest, therefore, that the data show a novel form of ROS scavenging in neonatal white matter vasculature, evolving over 15–20 min during a ROS challenge, persisting for 2–4 h.

ROS are implicated in a variety of CNS disorders (Traystman et al. 1991; Richardson, 1993), and their role has been highlighted in the formation of the white matter lesions of the developing brain that cause cerebral palsy. Cerebral palsy is the most common human birth disorder and is associated with high ROS levels in the CSF (Inder et al. 2002), and significant free-radical-mediated cell damage has been shown in post-mortem human sections (Back et al. 2005). Endothelial cells of the brain vasculature may be a major source of ROS (Zweier et al. 1988) and are also sensitive to the effects of ROS. For example, 100 μM H_2O_2 produces a rapid disruption of the tight junctions between endothelial cells that constitutes the blood-brain barrier (e.g. Shasby et al. 1985; Siflinger-Birnboim et al. 1996; Carbajal & Schaeffer, 1998; Kevil et al. 2001; Lee et al. 2004), although much higher concentrations are required to produce an acute effect upon endothelial cell viability. Exposure to ROS results in the activation of a variety of intracellular signalling pathways in endothelial cells, culminating in cell shape change and the loss of tight junctions (Shasby et al. 1985; Siflinger-Birnboim et al. 1996). At least one key event in the signalling pathways, protein tyrosine phosphorylation, is rapid in onset and transitory (Carbajal & Schaeffer, 1998; Kevil et al. 2001), while Ca^{2+} influx and phospholipase-D activation occurs after a $\sim$ 10–15 min delay (Shasby et al. 1985; Natarajan et al. 1996). A role for these cell signalling pathways in the rapid onset of ROS scavenging observed in the current study is suggested by the partially Ca^{2+}-dependent nature of the phenomena, while it is apparent that downstream cell signalling events with an appropriate time-course to actuate rapid scavenging are activated in the cells. Changes in the ability of cells to scavenge ROS have been described previously following exposure to free radicals, but never over such a rapid time-course. The speed of the effect precludes gene transcription and de novo protein synthesis and is similar in the time-course to an increase in catalase activity that has been reported in the CNS following stress (Islekel et al. 1999). It is known that catalase is highly expressed in developing white matter (Brannan et al. 1981) but inhibition of catalase failed to block the rapid scavenging of ROS and it

would appear that the phenomenon is not due to unregulated optic nerve catalase.

The concentration of H_2O_2 used in most of the experiments (100 μM) is comparable to the values reported in ischaemic and post-ischaemic brain (Hyslop et al. 1995) and is capable of injuring all cell types in the CNS (Whittemore et al. 1995; Desagher et al. 1996; Papadopoulos et al. 1998; Vollgraf et al. 1999; Roediger & Armati, 2003; Fragoso et al. 2004; Mazlan et al. 2006). The sole exception is vascular endothelial cells, which undergo shape change and loss of tight junction connections but do not die following exposure to this level of H_2O_2 (Shasby et al. 1985; Siflinger-Birnboim et al. 1996; Lee et al. 2004). The current findings suggest that vascular endothelial cells of white matter micro-vessels have a powerful mechanism capable of buffering the harmful ROS that are generated during acute ischaemia and other pathological states, a phenomenon that will contribute to the high resistance to oxidative injury in these cells.

Acknowledgement

References

Alix JJP, Fern R (2009) Glutamate receptor mediated ischemic injury of premyelinated central white matter. *Annals of Neurology* **66**, 682–693.

Back SA, Rivkees SA (2004) Emerging concepts in periventricular white matter injury. *Semin Perinatol* **28**, 405–414.

Back SA, Gan X, Li Y, et al. (1998) Maturation-dependent vulnerability of oligodendrocytes to oxidative stress-induced death caused by glutathione depletion. *J Neurosci* **18**, 6241–6253.

Back SA, Luo NL, Borenstein NS, et al. (2001) Late oligodendrocyte progenitors coincide with the developmental window of vulnerability for human perinatal white matter injury. *J Neurosci* **21**, 1302–1312.

Back SA, Luo NL, Mallinson RA, et al. (2005) Selective vulnerability of preterm white matter to oxidative damage defined by F2-isoprostanes. *Ann Neurol* **58**, 108–120.

Brannan TS, Maker HS, Raes IP (1981) Regional distribution of catalase in the adult rat brain. *J Neurochem* **36**, 307–309.

Braun A, Xu H, Hu F, et al. (2007) Paucity of pericytes in germinal matrix vasculature of premature infants. *J Neurosci* **27**, 12012–12024.

Carbajal JM, Schaeffer RC Jr (1998) H_2O_2 and genistein differentially modulate protein tyrosine phosphorylation, endothelial morphology, and monolayer barrier function. *Biochem Biophys Res Commun* **249**, 461–466.

Craig A, Ling Luo N, Beardsley DJ, et al. (2003) Quantitative analysis of perinatal rodent oligodendrocyte lineage progression and its correlation with human. *Exp Neurol* **181**, 231–240.

Daneman R, Zhou L, Kebede AA, et al. (2010) Pericytes are required for blood-brain barrier integrity during embryogenesis. *Nature* **468**, 562–566.

Desagher S, Glowinski J, Premont J (1996) Astrocytes protect neurons from hydrogen peroxide toxicity. *J Neurosci* **16**, 2553–2562.

Dringen R, Gutterer JM, Hirrlinger J (2000) Glutathione metabolism in brain metabolic interaction between astrocytes and neurons in the defense against reactive oxygen species. *Eur J Biochem* **267**, 4912–4916.

Fern R (1998) Intracellular calcium and cell death during ischemia in neonatal rat white matter astrocytes in situ. *J Neurosci* **18**, 7232–7243.

Foster RE, Connors BW, Waxman SG (1982) Rat optic nerve: electrophysiological, pharmacological and anatomical studies during development. *Brain Res* **255**, 371–386.

Fragoso G, Martinez-Bermudez AK, Liu HN, et al. (2004) Developmental differences in HO-induced oligodendrocyte cell death: role of glutathione, mitogen-activated protein kinases and caspase 3. *J Neurochem* **90**, 392–404.

Gerhardt H, Betsholtz C (2003) Endothelial-pericyte interactions in angiogenesis. *Cell Tissue Res* **314**, 15–23.

Gomes A, Fernandes E, Lima JL (2005) Fluorescence probes used for detection of reactive oxygen species. *J Biochem Biophys Methods* **65**, 45–80.

Hildebrand C, Waxman SG (1984) Postnatal differentiation of rat optic nerve fibers: electron microscopic observations on the development of nodes of Ranvier and axoglial relations. *J Comp Neurol* **224**, 25–37.

Hu Q, Xia Y, Corda S, et al. (1998) Hydrogen peroxide decreases pHi in human aortic endothelial cells by inhibiting Na+/H+ exchange. *Circ Res* **83**, 644–651.

Hyslop PA, Zhang Z, Pearson DV, et al. (1995) Measurement of striatal H_2O_2 by microdialysis following global forebrain ischemia and reperfusion in the rat: correlation with the cytotoxic potential of H_2O_2 in vitro. *Brain Res* **671**, 181–186.

Inder T, Mocatta T, Darlow B, et al. (2002) Elevated free radical products in the cerebrospinal fluid of VLBW infants with cerebral white matter injury. *Pediatr Res* **52**, 213–218.

Islekel S, Islekel H, Guner G, et al. (1999) Alterations in superoxide dismutase, glutathione peroxidase and catalase activities in experimental cerebral ischemia-reperfusion. *Res Exp Med (Berl)* **199**, 167–176.

Keller A, Mohamed A, Drose S, et al. (2004) Analysis of dichlorodihydrofluorescein and dihydrocalcein as probes for the detection of intracellular reactive oxygen species. *Free Radic Res* **38**, 1257–1267.

Kevil CG, Okayama N, Alexander JS (2001) H_2O_2-mediated permeability II: importance of tyrosine phosphatase and kinase activity. *Am J Physiol Cell Physiol* **281**, C1940–C1947.

Lee HS, Namkoong K, Kim DH, et al. (2004) Hydrogen peroxide-induced alterations of tight junction proteins in bovine brain microvascular endothelial cells. *Microvasc Res* **68**, 231–238.

Mark KS, Davis TP (2002) Cerebral microvascular changes in permeability and tight junctions induced by hypoxia-reoxygenation. *Am J Physiol Heart Circ Physiol* **282**, H1485–H1494.

Mattiasson G, Friberg H, Hansson M, et al. (2003) Flow cytometric analysis of mitochondria from CA1 and CA3 regions of rat hippocampus reveals differences in permeability transition pore activation. *J Neurochem* **87**, 532–544.

Mazlan M, Sue Mian T, Mat Top G, et al. (2006) Comparative effects of alpha-tocopherol and gamma-tocotrienol against hydrogen peroxide induced apoptosis on primary-cultured astrocytes. *J Neurol Sci* **243**, 5–12.

Metea MR, Newman EA (2006) Glial cells dilate and constrict blood vessels: a mechanism of neurovascular coupling. *J Neurosci* **26**, 2862–2870.

Motiejunaite R, Kazlauskas A (2008) Pericytes and ocular diseases. *Exp Eye Res* **86**, 171–177.

Mustapha NM, Tarr JM, Kohner EM, et al. (2010) NADPH oxidase versus mitochondria-derived ROS in glucose-induced apoptosis of pericytes in early diabetic retinopathy. *J Ophthalmol* **2010**, 746978.

Natarajan V, Vepa S, Verma RS, et al. (1996) Role of protein tyrosine phosphorylation in H_2O_2-induced activation of endothelial cell phospholipase D. *Am J Physiol* **271**, L400–L408.

Papadopoulos MC, Koumenis IL, Yuan TY, et al. (1998) Increasing vulnerability of astrocytes to oxidative injury with age despite constant antioxidant defenses. *Neuroscience* **82**, 915–925.

Peppiatt CM, Howarth C, Mobbs P, et al. (2006) Bidirectional control of CNS capillary diameter by pericytes. *Nature* **443**, 700–704.

Persidsky Y, Ramirez SH, Haorah J, et al. (2006) Blood-brain barrier: structural components and function under physiologic and pathologic conditions. *J Neuroimmune Pharmacol* **1**, 223–236.

Reynolds IJ, Hastings TG (1995) Glutamate induces the production of reactive oxygen species in cultured forebrain neurons following NMDA receptor activation. *J Neurosci* **15**, 3318–3327.

Richardson JS (1993) Free radicals in the genesis of Alzheimer's disease. *Ann N Y Acad Sci* **695**, 73–76.

Ridnour LA, Sim JE, Choi J, et al. (2005) Nitric oxide-induced resistance to hydrogen peroxide stress is a glutamate cysteine ligase activity-dependent process. *Free Radic Biol Med* **38**, 1361–1371.

Roediger B, Armati PJ (2003) Oxidative stress induces axonal beading in cultured human brain tissue. *Neurobiol Dis* **13**, 222–229.

Safiulina VF, Afzalov R, Khiroug L, et al. (2006) Reactive oxygen species mediate the potentiating effects of ATP on GABAergic synaptic transmission in the immature hippocampus. *J Biol Chem* **281**, 23464–23470.

Salter MG, Fern R (2005) NMDA receptors are expressed in developing oligodendrocyte processes and mediate injury. *Nature* **438**, 1167–1171.

Salter MG, Fern R (2008) The mechanisms of acute ischemic injury in the cell processes of developing white matter astrocytes. *J Cereb Blood Flow Metab* **28**, 588–601.

Sayre LM, Perry G, Smith MA (1999) In situ methods for detection and localization of markers of oxidative stress: application in neurodegenerative disorders. *Methods Enzymol* **309**, 133–152.

Scott TM, Foote J (1984) The postnatal development of blood vessels in the optic nerve of normotensive and hypertensive rats. *J Anat* **138**(Pt 4), 635–642.

Shannon C, Salter M, Fern R (2007) GFP imaging of live astrocytes: regional differences in the effects of ischaemia upon astrocytes. *J Anat* **210**, 684–692.

Shasby DM, Lind SE, Shasby SS, et al. (1985) Reversible oxidant-induced increases in albumin transfer across cultured endothelium: alterations in cell shape and calcium homeostasis. *Blood* **65**, 605–614.

Shepro D, Morel NM (1993) Pericyte physiology. *FASEB J* **7**, 1031–1038.

Siflinger-Birnboim A, Lum H, Del Vecchio PJ, et al. (1996) Involvement of Ca^{2+} in the H_2O_2-induced increase in endothelial permeability. *Am J Physiol* **270**, L973–L978.

Sims DE (1986) The pericyte – a review. *Tissue Cell* **18**, 153–174.

Sipos H, Torocsik B, Tretter L, et al. (2005) Impaired regulation of pH homeostasis by oxidative stress in rat brain capillary endothelial cells. *Cell Mol Neurobiol* **25**, 141–151.

Skoff RP, Price DL, Stocks A (1976) Electron microscopic autoradiographic studies of gliogenesis in rat optic nerve. II. Time of origin. *J Comp Neurol* **169**, 313–334.

Small RK, Riddle P, Noble M (1987) Evidence for migration of oligodendrocyte – type-2 astrocyte progenitor cells into the developing rat optic nerve. *Nature* **328**, 155–157.

Spitz DR, Dewey WC, Li GC (1987) Hydrogen peroxide or heat shock induces resistance to hydrogen peroxide in Chinese hamster fibroblasts. *J Cell Physiol* **131**, 364–373.

Thomas R, Salter MG, Wilke S, et al. (2004) Acute ischemic injury of astrocytes is mediated by Na-K-Cl cotransport and not Ca^{2+} influx at a key point in white matter development. *J Neuropathol Exp Neurol* **63**, 856–871.

Tirlapur UK, Konig K, Peuckert C, et al. (2001) Femtosecond near-infrared laser pulses elicit generation of reactive oxygen species in mammalian cells leading to apoptosis-like death. *Exp Cell Res* **263**, 88–97.

Traystman RJ, Kirsch JR, Koehler RC (1991) Oxygen radical mechanisms of brain injury following ischemia and reperfusion. *J Appl Physiol* **71**, 1185–1195.

Vaughn JE (1969) An electron microscopic analysis of gliogenesis in rat optic nerves. *Z Zellforsch Mikrosk Anat* **94**, 293–324.

Vollgraf U, Wegner M, Richter-Landsberg C (1999) Activation of AP-1 and nuclear factor-kappaB transcription factors is involved in hydrogen peroxide-induced apoptotic cell death of oligodendrocytes. *J Neurochem* **73**, 2501–2509.

Whittemore ER, Loo DT, Watt JA, et al. (1995) A detailed analysis of hydrogen peroxide-induced cell death in primary neuronal culture. *Neuroscience* **67**, 921–932.

Wiese AG, Pacifici RE, Davies KJ (1995) Transient adaptation of oxidative stress in mammalian cells. *Arch Biochem Biophys* **318**, 231–240.

Wilke S, Salter MG, Thomas R, et al. (2004) Mechanism of acute ischemic injury of oligodendroglia in early myelinating white matter: the importance of astrocyte injury and glutamate release. *J Neuropathol Exp Neurol* **63**, 872–881.

Yuan X, Chittajallu R, Belachew S, et al. (2002) Expression of the green fluorescent protein in the oligodendrocyte lineage: a transgenic mouse for developmental and physiological studies. *J Neurosci Res* **70**, 529–545.

Zweier JL, Kuppusamy P, Lutty GA (1988) Measurement of endothelial cell free radical generation: evidence for a central mechanism of free radical injury in postischemic tissues. *Proc Natl Acad Sci U S A* **85**, 4046–4050.